Canadian Metallurgical Quarterly, Vol 39, No 3, pp 269-280, 2000
© Canadian Institute of Mining, Metallurgy and Petroleum
Published by Canadian Institute of Mining, Metallurgy and Petroleum
Printed in Canada. All rights reserved

CHLORINATION OF MAGNESIUM CARBONATE IN A STIRRED TANK REACTOR

MARK KENNEDY[1] **and RALPH HARRIS**[2]

[1]Kidd Creek Division, Falconbridge Ltd., South Porcupine, Ontario
[2] Corresponding Author:
Mining and Metallurgical Engineering, McGill University, 3610 University Street,
Montreal, QC H3A 2B2

(Received May 1999; in revised form August 1999)

Abstract — The rates of the chlorination reaction that occurred between a suspension of magnesium oxide and gas mixtures containing chlorine, carbon monoxide and nitrogen were measured when the gases were injected into a mechanically agitated molten salt bath containing the suspension. The magnesium oxide suspension was formed in situ when dried magnesium carbonate was added to the molten bath. Rates of chlorination were measured over a range of temperatures from 740 to 910 °C, total gas flow rates from 3 to 11 x 10^{-5} m^3/s STP, CO/Cl_2 ratios from 0.67:1 to 1.6:1, nitrogen dilutions from 0 to 75 v/v%, iron additions from 0 to 560 PPM and impeller speeds from 250 to 1150 rpm. The chlorination reaction exhibited an activation energy of 80 kJ/mol over the temperature range from 740 to 825 °C and the fastest chlorination was found to be at a temperature of 860 °C and a CO/Cl_2 ratio of 1.2:1. The chlorination rate was found not to depend on MgO concentration in the melt or on the MgO particle size indicating that the rate controlling step was not at the particle / melt interface. Experiments at different CO/Cl_2 ratios and constant gas flow rate indicated that it was transfer of CO rather than transfer of Cl that determined the chlorination rate. Experiments at constant CO/Cl_2 ratios and increasing nitrogen dilution found decreasing rates of chlorination. Iron additions to the melt were found to have no effect. For experiments that were carried out at 820 °C, the rate of chlorination was correlated as:

$$\tilde{R}_{MgO} = 1.69x10^{-4}\left(\frac{P_{gassed}}{V_{liquid}}\right)^{0.35} v_g^{0.64} p_{CO}^{1.14} \frac{kmol}{m^3 s}$$

Résumé — On a mesuré le taux de réaction de chloration entre une suspension d'oxyde de magnésium et des mélanges gazeux contenant du chlore, du monoxyde de carbone et de l'azote, au moment où l'on injectait les gaz dans un bain de sel fondu agité mécaniquement et contenant la suspension. La suspension d'oxyde de magnésium se formait in situ quand on ajoutait au bain fondu du carbonate de magnésium séché. On a mesuré les taux de chloration sur une gamme de températures allant de 740 à 910 °C, avec des taux d'écoulement total de gaz de 3 à 11 x 10^{-5} m^3/s STP, à des rapports de $CO/C1_2$ allant de 0.67:1 à 1.6:1, avec des dilutions d'azote de 0 à 75% v/v%, des additions de fer de 0 à 560 ppm et avec des vitesses d'hélices de 250 à 1150 rpm. La réaction de chloration exhibait une énergie d'activation de 80 kJ/mol pour la gamme de température allant de 740 à 825 °C et la chloration la plus rapide s'est produite à une température de 860 °C, avec un rapport de $CO/C1_2$ de 1.2:1. On a trouvé que le taux de chloration ne dépendait pas de la concentration de MgO dans le bain fondu ni de la taille de particule de MgO, indiquant que l'étape de contrôle du taux ne se trouvait pas à l'interface particule/bain fondu. Les expériences avec différents rapports de $CO/C1_2$ et à taux constant d'écoulement de gaz ont indiqué que c'était le transfert du CO plutôt que le transfert du CI qui déterminait le taux de chloration. Les expériences avec rapport constant de $CO/C1_2$ et une augmentation de la dilution de l'azote ont montré des taux décroissants de la chloration. Des additions de fer dans le bain fondu n'avaient pas d'effet. Pour les expériences conduites à 820 °C, le taux de chloration était corrélé à:

$$\tilde{R}_{MgO} = 1.69x10^{-4}\left(\frac{P_{gassed}}{V_{liquid}}\right)^{0.35} v_g^{0.64} p_{CO}^{1.14} \frac{kmol}{m^3 s}$$

Published by Maney Publishing (c) Canadian Institute of Mining, Metallurgy and Petroleum

Published by Maney Publishing (c) Canadian Institute of Mining, Metallurgy and Petroleum

INTRODUCTION

Magnesium occurs naturally in a number of solid compounds, as dolomite, $MgCO_3.CaCO_3$, magnesium carbonate (also known as magnesite), $MgCO_3$, carnallite, $MgCl_2.KCl.6H_2O$, serpentine, $Mg_6(OH)6Si_4O_{11}.H_2O$, and magnesium chloride, $MgCl_2$, which occurs dissolved in sea water as well as surface and underground brines. $MgCl_2$ is the earth's eighth most abundant element. Magnesium has high strength and stiffness to weight ratios making it suitable as a structural metal and, in the absence of certain impurities, magnesium has a greater corrosion resistance than aluminum. Magnesium presently finds applications principally as an alloying agent for aluminum (49%), as an iron and steel desulphurizer (21%) and in pressure die castings (18 %). World production of magnesium was 303,000 tons in 1993, which was roughly 2 % of the world production of aluminum [1]. About 75% of the world's magnesium is presently produced by electrolysis of a mixed fused salt ($MgCl_2$ / KCL / NaC_l) and the remainder is produced by metallothermic reduction with ferrosilicon in vacuum retorts [2] or via the Magnetherm process [3]. For the electrolysis route, the naturally occurring minerals, with the exception of $MgCl_2$, are converted to magnesite and then chlorinated [4,5,6]. The resulting magnesite is contaminated with hydrates and magnesium oxide which, if not removed, result in yield losses and operational problems during electrolysis. The present study [7] is concerned with the production of magnesium chloride by chlorination of magnesium carbonate added to a mechanically agitated bath of molten $MgCl_2$ using carbon monoxide / chlorine / nitrogen gas mixtures. The resulting molten $MgCl_2$, containing little or no oxide, could be used as feed for fused salt electrolysis without the associated operational problems associated with conventional sources of $MgCl_2$.

THERMODYNAMICS AND KINETICS

The steps in the chlorination process [8] which involved thethermal decomposition of magnesium carbonate are:

$$\begin{aligned} MgCO_3 &= MgO + CO_2 \\ \Delta G^\circ\Big|_{723}^{1223} &= 0.159T + 62.43 kJ / mol \end{aligned} \quad (1)$$

and the reduction and chlorination of the oxide:

$$\begin{aligned} MgO + CO + CI_2 &= MgI_2 + CO_2 \\ \Delta G^\circ\Big|_{723}^{1223} &= 0.103T - 263.1 kJ / mol \end{aligned} \quad (2)$$

The rate of the second step has been suggested to be determined by the rate of CO transfer in the liquid molten salt phase when MgO was suspended in molten $MgCl_2$ [9]. Consequently, the chlorination rate would depend on the gas / liquid contact area, the liquid phase mass transfer coefficient for CO transfer and the activity difference between the source and the sink of CO, i.e.:

$$\tilde{R}_{MgO} = a k_I \left(C^*_{CO} - C^b_{CO} \right) \text{ kmol m}^{-3}\, s^{-1} \quad (3)$$

The bracketed term reflects the difference between the activity of CO at the liquid/gas interface and the activity of CO in the bulk liquid. Activity is expressed here as concentration, i.e., kmol m^{-3}, implying that the activity coefficient of CO dissolved in the molten salt was independent of concentration. It was also assumed that the CO activity at the interface was proportional to the CO partial pressure with the result that it was anticipated that the chlorination rate would be proportional to the CO partial pressure.

An estimate of the liquid phase mass transfer coefficient for mass transfer from spherical bubbles, in the absence of chemical enhancement, can be obtained from [10]:

$$N_{Sh} = \frac{k_I d_b}{D_I} = 2.0 + 0.31 N_{Ra}^{1/3} \quad (4)$$

When the equivalent bubble diameter is less than about 1.4 mm [10], the bubbles are roughly spherical and the gas / liquid interfacial area per unit volume, i.e., the specific gas surface area, a, can be calculated from the mean bubble diameter and the gas hold-up, i.e.:

$$a = \frac{6\varepsilon}{d_b} \quad (5)$$

The gas hold-up, ε, is the fraction of the total dispersion occupied by gas, i.e.:

$$\varepsilon = \frac{V_{total} - V_{liquid}}{V_{total}} \quad (6)$$

Many correlations for the gas hold-up for different impeller designs are available in the literature [11], for example:

$$\varepsilon = 17.9 \left(\frac{P_{gassed}}{V_{liquid}} \right)^{0.31} v_g^{0.67} \quad (7)$$

Published by Maney Publishing (c) Canadian Institute of Mining, Metallurgy and Petroleum

or

$$\varepsilon = 0.52\, N_a^{0.5}\, N_{We}^{0.65} \left(\frac{d_{impeller}}{d_{vessel}} \right)^{1.4} \tag{8}$$

Since the impeller used in the present work was not a standard design and little is known about the behaviour of gas bubbles in agitated fused salt baths, the following general expression for the chlorination rate constant was assumed to characterize the overall rate behaviour:

$$k_l a \propto \left(\frac{P_{gassed}}{V_{liquid}} \right)^x v_g^y \tag{9}$$

Such a characterization followed from the assumptions that could be made about the activity of CO at the gas / liquid interface and in the bulk molten electrolyte [12,13]:

Previous studies at 20°C on coalescing systems (pure water) and non-coalescing systems (water / aqueous electrolyte) have determined the following correlation, respectively [12], for the chlorination rate constant:

$$k_l a = 2.3 \left(\frac{P_{gassed}}{V_{liquid}} \right)^{0.7} v_g^{0.6} \tag{10}$$

$$k_l a = 1.2 \left(\frac{P_{gassed}}{V_{liquid}} \right)^{0.7} v_g^{0.6} \tag{11}$$

Other studies have found that the rate of alkali metal chlorination in molten aluminum when a rotary gas injector was used, depended on the operating conditions and system dimensions as follows [14]:

$$R \propto \left(\frac{N^3 d_{impeller}^5}{V_{liquid}} \right)^{0.105} v_g^{1.14} \tag{12}$$

It is interesting to note that the exponent of the superficial gas velocity for the liquid metal study was significantly different from those in the water studies.

EXPERIMENTAL

The objectives of the experiments were:

1. to determine the rate of chlorination of magnesite suspended in molten magnesium chloride when CO / Cl_2 mixtures were injected via a rotating submerged impeller,
2. to infer the rate controlling step from the experimental results and
3. to quantify the effect of the process parameters, namely, reaction gas flow rate, reaction gas composition, temperature, impeller speed, iron addition and dilution of the reaction gas with nitrogen.

The experimental set-up is shown schematically in Figure 1. A three-phase 40 kVA "glowbar" resistance furnace was used to maintain the temperature of the reaction vessel which was comprised of a silicon carbide, Morganite EF 444 Salamander crucible (OH 0.476 m, IH 0.451 m, OD 0.254 m, ID 0.216 m) holding a graphite (Speer -890S) crucible (OH 0.33 m, IH 0.30 m, OD 0.20 m, ID 0.16 m). The graphite crucible was equipped with four graphite (UCAR-ATJ) baffles (0.25m high, 0.012 m thick and 0.025 m wide) that were countersunk 0.0095 m into 0.0125 m wide slots in the crucible wall at 90° intervals and held in place using graphite cement (UCAR C-34).

Table II summarizes the dimensions of the experimental apparatus and Table III summarizes the experimental conditions:

The impeller speed was measured with a Shimpo optical tachometer, Model Dt 205B, and controlled with an Emerson Industrial Controls, Focus 2, Model PN2450-8000, direct current speed controller. Mixing power was determined by measuring the difference in the armature voltage and current using two Meter Master, Model RP-35V, meters between tests with the impeller submerged and not submerged in the fused salt. Bath and furnace temperatures were measured using type K thermocouples housed in 0.003 m by 0.61m long stainless steel sheaths. Vycor glass tubes, sealed at one end, were used to protect the stainless steel thermocouple sheaths from the corrosive environment of the reactor. Gas flow was measured with Gilmont

Table II – Dimensions of the Experimental Apparatus

Dimension	Value (m)
reactor diameter	0.159
molten bath depth	0.165
impeller diameter	0.076
impeller thickness	0.038
impeller distance from bottom	0.038
baffle width	0.016
liquid height above impeller	0.089
impeller shaft diameter	0.038
impeller bore diameter	0.006
distance of gas holes from impeller base	0.013
width of slots in impeller	0.0115

Table III — Experimental Conditions (Gas flows at STP)

Exp No.	MgO Particle Size, μ		Temp	σ T	RPM	Cl_2 x 10^5	CO x 10^5	N_2 x 10^5	Initial H x 10	Initial MgO	Initial Fe
	+	-	°C	°C		m^3/s	m^3/s	m^3/s	m	Wt %	PPM
1	53	75	829	3.39	1006	3.06	3.10	0.00	1.68	4.34	223
2	53	75	850	7.46	1005	2.34	2.42	0.00	1.73	5.26	351
3	212	300	815	14.69	1005	2.39	2.40	0.00	1.63	4.76	403
4	212	300	823	2.78	1003	3.05	3.09	4.71	1.7	5.07	349
5	212	300	821	5.15	1003	3.05	3.09	0.00	1.7	4.45	214
6	212	300	826	4.3	1005	1.56	1.56	0.00	1.7	4.77	232
7	53	75	821	3.1	1004	2.36	2.49	0.00	1.52	4.95	300
8	212	300	824	2.05	1004	0.78	0.77	0.00	1.65	5.12	255
9	212	300	823	2.11	1004	4.73	4.69	0.00	1.65	5.1	256
10	150	212	908	4.72	1005	3.04	3.11	0.00	1.65	4.65	239
11	150	212	743	3.57	1006	3.07	3.11	0.00	1.52	4.21	306
12	150	212	864	3.84	1005	3.04	3.11	0.00	1.78	4.01	264
13	150	212	783	1.34	1006	3.06	3.11	0.00	1.73	5.13	303
14	150	212	824	2.26	1004	3.07	3.11	0.00	1.63	3.85	222
15	106	150	824	4.81	1004	3.05	3.11	0.00	1.65	4.21	227
16	106	150	823	4.11	1004	2.36	2.50	1.65	1.68	3.46	252
17	106	150	823	3.41	1004	1.55	1.56	3.14	1.68	2.98	249
18	106	150	826	2.88	1004	1.56	1.56	0.00	1.63	3.69	245
19	106	150	825	2.62	1006	2.35	2.50	0.00	1.63	3.62	279
20	106	150	825	1.73	1004	0.79	0.79	0.00	1.73	3.64	308
21	106	150	824	3.57	1004	0.78	0.79	4.71	1.6	5.02	333
22	75	106	824	2.97	1004	3.06	3.11	0.00	1.63	4.06	227
23	75	106	825	2.45	1156	3.06	3.11	0.00	1.63	2.71	218
24	75	106	824	1.27	609	3.05	3.11	0.00	1.63	3.27	251
25	75	106	824	1.67	804	3.04	3.11	0.00	1.57	3.15	213
26	75	106	824	2.31	1006	3.06	3.11	0.00	1.63	4.01	441
27	75	106	825	1.57	1006	3.06	3.11	0.00	1.63	3.45	560
28	53	75	824	1.82	1002	3.05	3.11	0.00	1.68	2.32	232
29	53	75	824	2.21	1006	2.36	2.50	0.00	1.63	2.51	312
30	106	150	825	1.13	1004	3.71	2.50	0.00	1.65	3.69	202
31	106	150	824	2.38	1002	2.51	3.70	0.00	1.6	3.78	241
32	106	150	823	1.97	1005	2.37	3.70	0.00	1.65	3.02	296
33	106	150	823	1.69	1005	3.05	3.10	0.00	1.63	3.76	396

rotameters fitted with glass floats as follows: CO - #2-23335, Cl_2 - #2-R686 or #3-61664, N_2 #3-31627. Flow meters were calibrated using a GCA Precision Scientific, wet gas flow meter with the Gilmont flow rate analysis software, Model GF-4000 V1.0.

Ten kilograms of natural magnesite from the Baymag deposit [15] (-0.050 m - Lot #225062) were crushed by jaw and roll crushers to -0.006 m and then pulverized to obtain a uniform feed. It was then screened (Tyler screen sizes: 50, 70, 100, 140, 200 and 270) to obtain its particle size distribution. Chemical analysis of the various size fractions is presented in Table IV showing that the impurities tended to report to the larger size fractions.

An initial bath of magnesium chloride was formed by melting five kilograms Aldrich anhydrous magnesium chloride (formula weight 95.22, melting point 714 °C, SG

Published by Maney Publishing (c) Canadian Institute of Mining, Metallurgy and Petroleum

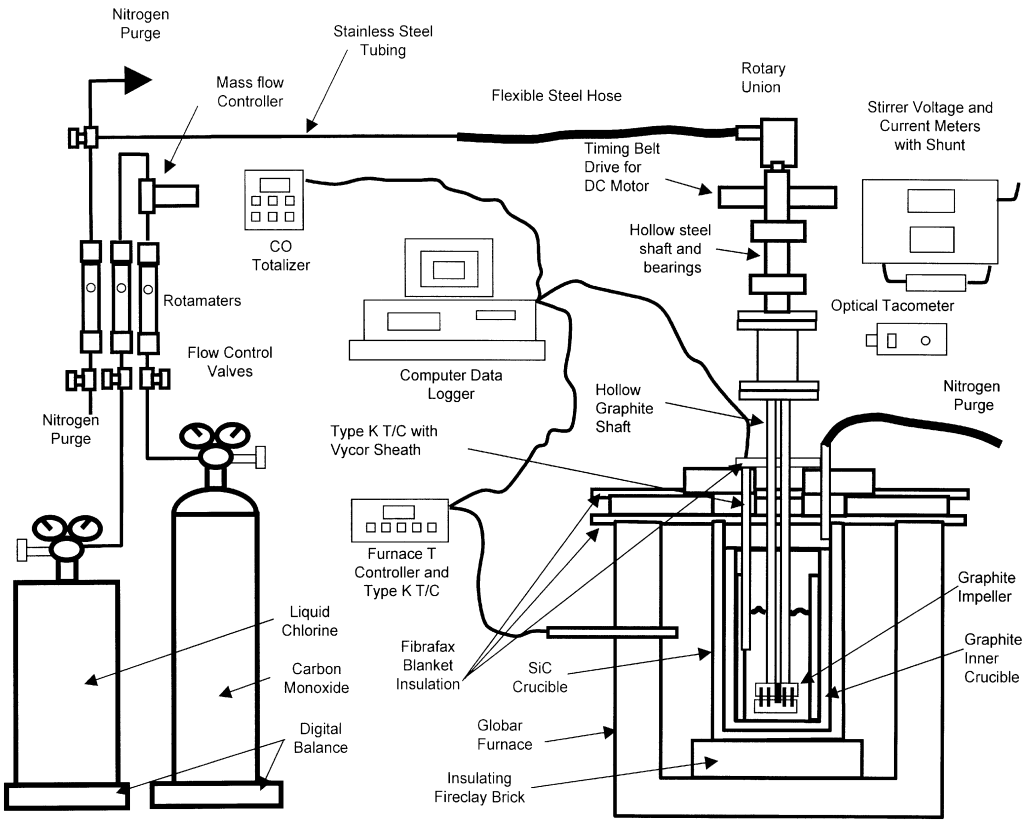

Fig. 1. Schematic Diagram of Experimental Set-up.

2.320, particle size -20 μm, lot number 10204AF, guaranteed less than 5 % moisture). Tests by the present authors found this material to be less than 1 wt % moisture by Karl Fischer titration. A chemical assay is given in Table V.

High purity chlorine (Matheson HP grade {> 99.5 %}) and compressed carbon monoxide (Praxair CP grade {> 99.5 %}) were used to form the reaction gases. Commercial liquid nitrogen (Praxair equivalent to extra dry nitrogen) was used as the diluent gas.

The experimental procedure was as follows. The depth of the molten $MgCl_2$ bath was measured by inserting a glass rod to the base of the molten bath several times and examining the length of material frozen on it. The level was adjusted as required to maintain the same initial level for all experiments. Thereafter, 0.3 to 0.6 kg of pre-dried (200 °C for 1 hour) $MgCO_3$ was added to the bath to yield a nominal initial MgO content of 2.5 to 5 wt %. The melt temperature was then adjusted to roughly 10 °C less than the set point and once the bath had stopped fuming, i.e., CO_2 evolution was complete, the rotary impeller / gas injector was lowered to its operating position with nitrogen flowing through it to prevent the molten bath from entering the gas passages, freezing and plugging them. The melt level was again measured and the impeller rotation started. Three (3) thirty to fifty gram melt samples were then taken in succession after a delay of 10 minutes to allow the system to homogenize using a 0.007 m OD Vycor tube and pipette bulb. A second sample was taken after another delay of 10 minutes and divided into two equal parts, one of which was subjected to a simple bench test to roughly determine the initial MgO content and the other stored for later rigorous chemical analysis. The bench test consisted of taking about 25 gm of the melt sample and weighing it precisely to +/- 0.0001 gm. This material was then dissolved in roughly 500 ml of water and the insoluble MgO was filtered out using a preweighed filter paper. The filter paper and MgO were heated at 150 °C for 10 minutes and reweighed. The MgO content was then taken as the increase in the weight divided by the initial sample mass.

The chlorine, carbon monoxide and nitrogen, if required, were then started if the initial MgO content was satisfactory, otherwise more magnesite was added and the procedure above repeated. Duplicate samples were taken thereafter at one hour intervals and the MgO content checked each time by the rough bench test until the MgO content was less than 0.1 wt %. One final sample was taken after another one hour delay. The final bath depth was also measured.

Published by Maney Publishing (c) Canadian Institute of Mining, Metallurgy and Petroleum

Table IV — Assay of Size Fractions of Pulverized and Screened Baymag Magnesite

Size (μm)	Ca %	Na PPM	K PPM	Si PPM	Al PPM	B PPM	Cu PPM
<53	0.66	973	109	747	353	28	1600
53-75	0.68	N/A	N/A	438	166	74	118
53-75	0.5	636	<100	460	252	29	954
75-106	0.49	557	<100	152	187	22	706
106-150	0.46	464	<100	105	151	18	485
150-212	0.46	291	<100	104	84	17	141
212-300	0.49	247	<100	83	82	21	67

Size (μm)	Fe %	Ni PPM	Cd PPM	Pb PPM	Mn PPM	Sb PPM
<53	0.3	30	N/A	237	118	85
53-75	0.2	2	<0.5	25	120	59
53-75	0.23	17	N/A	150	96	73
75-106	0.21	14	N/A	153	95	62
106-150	0.19	13	N/A	113	91	56
150-212	215	5	N/A	77	82	55
212-300	0.12	6	N/A	6	77	56

Table V — Assay of As-received Aldrich Anhydrous $MgCl_2$

Sample	MgO %	H_2O %	Ca PPM	Na PPM	K PPM	Li PPM	Al PPM
1	0.14	0.63/0.66	N/A	N/A	N/A	N/A	N/A
2	0.04	1.05/0.94	N/A	N/A	N/A	N/A	N/A
3	0.17	1.07/1.05	0.44/0.39	3.6/3.8	30/39	0.1/0.1	4.1/4.1

At the end of the experiment, the impeller was raised out of the bath and the power to the furnace was stopped and the bath allowed to cool and freeze in the graphite crucible under a flow of nitrogen. The bath was reused until the graphite crucible needed to be changed due to wear and tear and / or oxidation.

The MgO content of the samples was also determined by back titration. In this procedure, three gram samples were dissolved in water and 10 ml of 1N HCl were added to dissolve the MgO. The residual acid was titrated with 0.5 N NaOH to determine the amount of acid consumed and hence the MgO content. Minor elements were analysed by inductively coupled plasma spectrophotometery of solution of the samples dissolved in acid.

RESULTS

Impeller motor power draws were measured for an unused impeller, unsubmerged and submerged in a fresh $MgCl_2$ bath at 600, 800 and 1000 rpm at approximately 830 °C, for total gas flow rates of Cl_2 and CO ($CO:Cl_2$ = 1:1) of 1.0, 2.0, 3.0, 4.0 and 5 slpm. Mixing power was calculated as the difference between the unsubmerged and submerged impeller motor power draws. Figure 2 shows the power measurements and Figure 3 presents the ratio of gassed to ungassed power for the three impeller speeds and five gas flow rates plotted against the impeller aeration number. The three sets of data were correlated to yield:

$$\frac{P_{gassed}}{P_{ungassed}} = 0.452 \left(\frac{Q_{total}}{N\, d_{impeller}^3} \right)^{-0.22} \quad r^2 = 0.885 \quad (13)$$

Published by Maney Publishing (c) Canadian Institute of Mining, Metallurgy and Petroleum

The exponent in Equation 13 falls within the anticipated range, -0.22 to -0.38 [11,16] for six bladed turbines.

Figure 4 is a plot of the measured data for a typical experiment. The molar consumption rate of MgO was derived from the slope of the least squares regression of a plot of weight percent MgO remaining in the bath versus time, i.e.:

$$\tilde{R}_{MgO} = \overline{\left(\frac{\Delta wt\%MgO}{\Delta time}\right)} \frac{1}{100} \frac{\overline{\rho}_{bath}}{40.305} \left(\frac{kmol}{m^3 s}\right) \quad (14)$$

The average density of the bath was calculated from the weighted average of the MgO and MgCl2 densities:

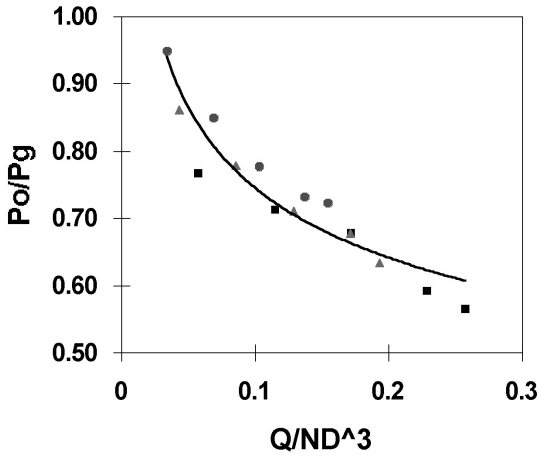

Fig. 3. Ratio of Ungassed to Gassed Impeller Power Draw versus Aeration Number (Q/ND_3). All data for 600, 800 and 1000 RPM included.

$$\overline{\rho}_{bath} = \frac{\left[\left(\rho^{liquid}_{MgCl_2}(100 - wt\%MgO) + \rho^{solid}_{MgO} wt\%MgO\right)_{initial} + \left(\rho^{liquid}_{MgCl_2}(100 - wt\%MgO) + \rho^{solid}_{MgO} wt\%MgO\right)_{final}\right]}{200} \quad (15)$$

Table VI summarizes the experimental results for the thirty-three experiments performed. Gas hold-up measurements were difficult due to the proximity of the rotating impeller and the instability of the bath surface during gas injection. The gas hold-up results are therefore only an indication of the behaviour of the system and are not dealt with further. The times listed in Table VI are the duration of gas injection. The reaction efficiencies of the CO and Cl_2 were calculated from the molar flow rate of the gases, the average bath volume and the measured molar MgO consumption rate, i.e.

$$Eff_{gas^\circ} = \tilde{R}_{MgO} \frac{\overline{V}_{bath}}{\tilde{Q}_{gas}} 100 \quad (16)$$

The mixing power correlations above were used with experimental conditions, i.e., impeller speeds, gas flow rates and gas compositions to develop an expression for the chlorination rate, i.e.:

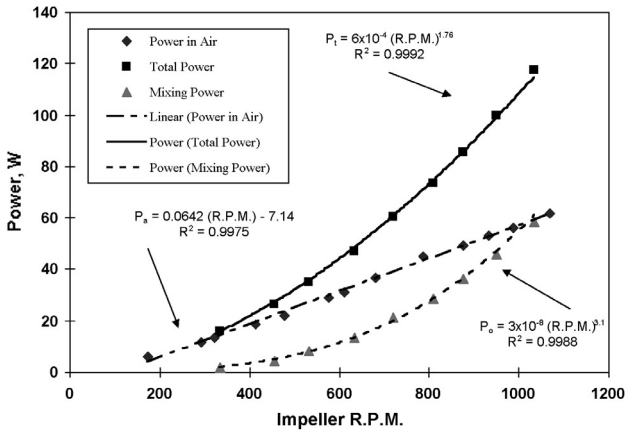

Fig. 2. Measured impeller power draws versus impeller RPM.

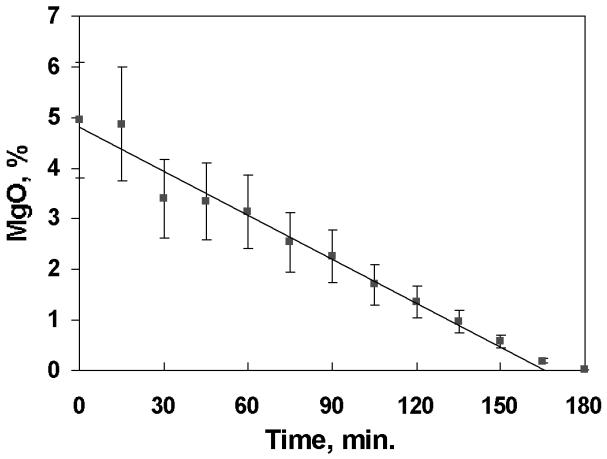

Fig. 4. Measured MgO content versus time for a typical experiment; Exp. 7.

Published by Maney Publishing (c) Canadian Institute of Mining, Metallurgy and Petroleum

Table VI — Experimental Results

Exp No.	R_{MgO} x10^4 kmol/m^3/s	+/- %	Utilization Cl_2 %	Utilization CO %	Gas hold-up %	Time x10^{-3} s	Efficiency Cl_2 %	Efficiency CO %
1	3.44	7	115	96	8.3	7.32	80	80.6
2	2.81	13.1	84	122	11.6	9.9	88.9	86.3
3	2.33	12.5	112	92	10	9.9	68.4	67.9
4	1.22	9.7	103	109	21.9	17.1	27.5	27
5	1.97	16.9	102	87	5.2	10.8	47.5	46.7
6	1.69	10.6	N/A	N/A	3.6	15.36	73.9	73.8
7	2.03	13.2	106	99	6	11.76	54.4	51.4
8	0.78	4.8	100	100	8.3	28.5	60.8	59.8
9	2.83	30.1	104	108	16.7	10.8	40.5	40.8
10	2.72	35.4	105	115	4.5	8.1	63.6	61.3
11	1.53	9.9	102	111	0	12.6	34	33.6
12	2.92	51.7	109	88	13.2	7.98	73.7	72.1
13	3.08	5.7	102	106	17.9	9.9	73.4	72.2
14	2.22	4.7	98	N/A	7	11.7	50.3	49.7
15	2.42	7.8	105	104	14.3	9	56.3	55.1
16	1.69	15.2	112	87	9.8	11.7	51.9	49
17	1.08	16.2	100	101	14.3	16.2	50	50
18	1.78	11.4	95	99	15.9	11.7	79.4	79.4
19	1.94	10.2	102	97	13.1	9	57.7	54.4
20	1.03	6.1	101	102	8.9	18	90.6	89.9
21	0.56	16.2	106	102	5.1	27	47.2	46.4
22	2.42	22.3	100	106	10.8	9.9	55	54.1
23	1.94	26	98	97	16.1	7.2	44	43.3
24	1.22	11.7	99	95	8.8	13.5	28	27.5
25	1.22	10.7	109	110	9.6	11.7	26.8	26.2
26	1.92	18.9	102	94	10.1	9.9	44.1	43.4
27	1.97	19	99	101	7	8.1	45.3	44.6
28	1.36	18.2	105	114	3.4	7.2	32.8	32.2
29	1.47	18.3	81	81	4.5	9	43.7	41.3
30	1.17	24.4	100	100	N/A	11.7	22.3	33.2
31	2.86	28.9	125	125	6.9	6.3	79.2	55.7
32	2.25	11.1	91	91	N/A	5.4	68.5	43.8
33	2.97	20.1	112	112	4.2	6.3	69.6	68.3

$$\tilde{R}_{MgO} = 1.69x10^{-4}\left(\frac{P_{gassed}}{V_{liquid}}\right)^{0.35} v_g^{0.64} p_{CO}^{1.14} \frac{kmol}{m^3 s} \quad (17)$$

DISCUSSION

The observation that the chlorination rate of MgO particles was found to be independent of the amount of MgO in suspension (see Table III) meant that the removal was "zero order" with respect to MgO concentration and indicated that the rate controlling process was mass transfer at the gas / liquid interface and not at the liquid / particle interface. It was also found that iron additions to the melt, which may have increased the ionic transport rates by exchange

Published by Maney Publishing (c) Canadian Institute of Mining, Metallurgy and Petroleum

Published by Maney Publishing (c) Canadian Institute of Mining, Metallurgy and Petroleum

between Fe^{2+} and Fe^{3+}[17], had no effect on the rates of chlorination.

Figure 5 shows that the rate of chlorination of the MgO increased with increasing total flow rate of gas for both size fractions tested at 830 °C. It also approached a maximum which would seem to be reasonable since it would be expected that the impeller would tend to flood and provide poorer mixing and poorer gas dispersion at the higher flow rates. Over the range examined, a curve was fitted to the data in Figure 5, i.e.:

$$\tilde{R}_{MgO} = 0.0053\, Q_{total}^{0.63} \quad r^2 = 0.866 \qquad (18)$$

Since the chlorination rate was proportional to the rate constant, the exponent of the gas flow rate can be compared to that for the superficial gas velocity versus the rate constant for mass transfer in other gas contacting situations. There was reasonable agreement with previous studies on oxygenation of aqueous systems in stirred tank reactors [18] for which the exponent was approximately 0.5.

It was found that there is no obvious pattern amongst the chlorination rate data with respect to particle size, Table III, a behaviour which also indicated that the rate controlling step was not at the liquid / particle interface. Since the chlorination rate was independent of the MgO content and the
particle size, then it must also have been independent of all other properties of the MgO particles such as porosity and actual and apparent surface area.

Most of the experiments were performed with the stoichiometric ratio of CO / Cl_2, i.e., 1:1. However, the present study was also interested in examining ways to increase the rate, so tests were performed that were biased towards higher CO concentrations because it was thought that this was the most likely way to increase the rate of chlorination. Consequently, there was only one data point at a CO / Cl_2 ratio less than stoichiometric, Figure 6. Nevertheless, it would appear that the rate of chlorination fell off faster with a decrease in CO content than with a decrease in Cl_2 content suggesting that it was the transfer of CO rather than the transfer of Cl_2 that was rate limiting. This was in agreement with previous work [9], Figure 7, which also showed that an optimum CO / Cl_2 ratio existed for the chlorination of MgO suspended in $MgCl_2$. The present results indicate that an optimum existed at around a CO:Cl_2 ratio of 1.2:1.

Two series of experiments were carried out with increasing levels of dilution of the reaction gases with nitrogen to determine whether the gas / liquid interfacial area or the reaction gas activity was more significant in controlling the rate of the chlorination. The results of the experiments with constant total gas flow rate, i.e., constant specific surface area, are shown in Figure 8. It can be seen that as the dilution increased, the chlorination rate and the CO and Cl_2 efficiencies decreased indicating that diffusion

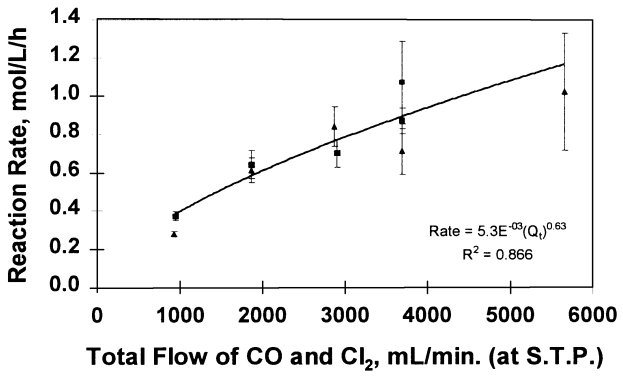

Fig. 5. Chlorination rate versus total injected gas flow rate from Tables III and VI.

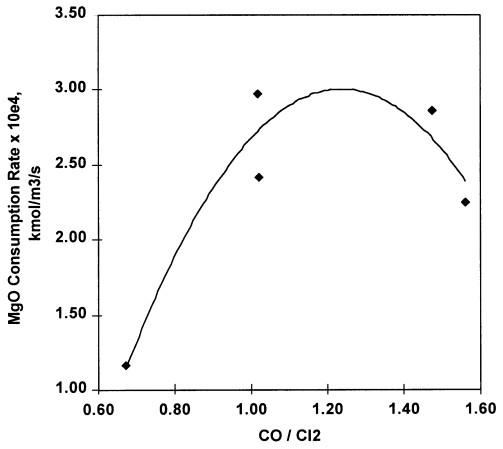

Fig. 6. Rate of MgO consumption versus CO/Cl_2 from Table VI.

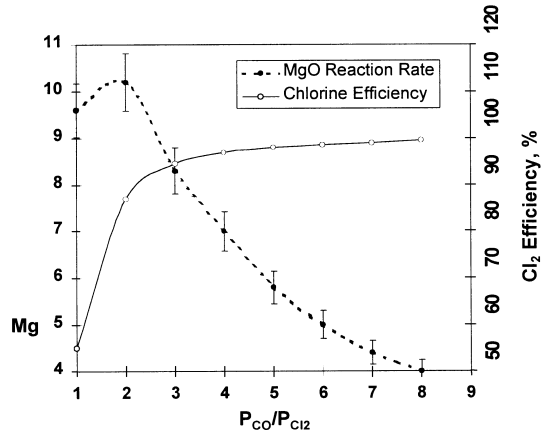

Fig. 7. Experimental results of Pruttskov [9].

from the gas phase into the liquid phase was the rate controlling step. The chlorination rate was correlated against nitrogen dilution as follows:

$$\tilde{R}_{MgO} = 0.943 - 0.11\ v/v\%N_2 \quad r^2 = 0.942 \qquad (19)$$

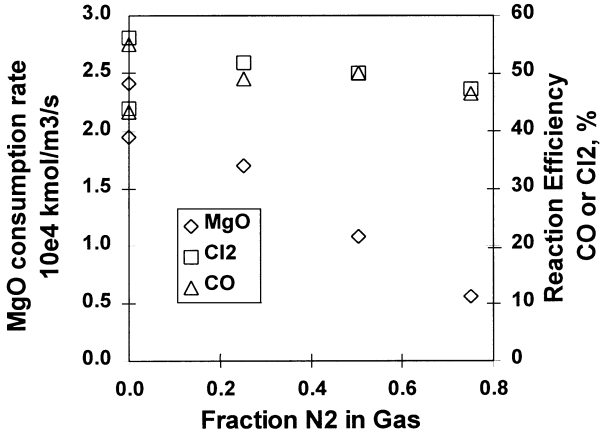

Fig. 8. Rate of MgO Consumption and CO and Cl_2 Utilization Efficiency versus the fraction of N_2 in the injected gases from Table VI.

The results of the experiments with constant CO plus Cl_2 flow rate and increasing nitrogen flow rate, i.e., constant CO and Cl_2 partial pressures but increasing specific surface area, are shown in Figure 9. It can be seen that the relative rate of chlorination, i.e., rate undiluted over rate diluted, decreased as the concentration of nitrogen increased providing further confirmation that the rate controlling step was from the gas phase to the liquid phase. Figure 9 shows that there is no advantage to be gained by diluting the reaction gases with an inert gas to increase the specific surface area.

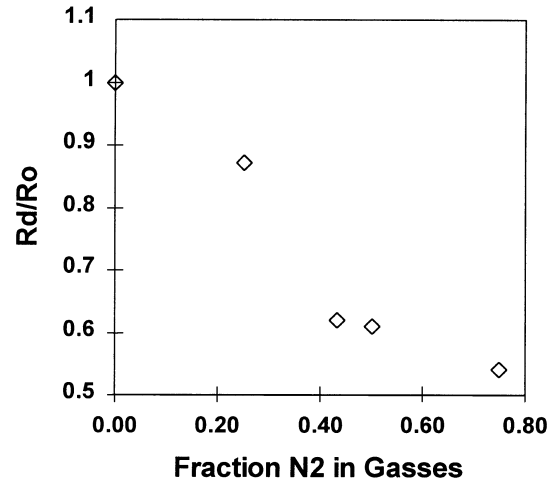

Fig. 9. Ratio of chlorination rate with reaction gases diluted and reaction gases undiluted, versus fraction of N_2 in injected gasses from Table VI.

The overall expression for the chlorination rate, Equation 17, shows that the exponent of the mixing power per unit volume term was significantly lower than that for aqueous systems, Equations 10 and 11, whereas the exponent of the superficial gas velocity was roughly the same. The lower value of the exponent of the mixing power per unit volume means that there is less benefit to be had by increasing the mixing power per unit volume as compared to aqueous systems. One possible reason for this is that the gas bubble population was fairly uniform in size and the size was not easily reduced by more intense agitation. This observation warrants further investigation if this method of chlorination is to be exploited on a commercial scale.

Increasing superficial gas velocity increased the specific surface area which in turn increased the rate of reaction. The exponent of the CO partial pressure was roughly one which was in good agreement with the assumption that the CO activity at the gas / liquid interface was proportional to the CO partial pressure in the bubble.

SUMMARY

The present experiments have found that the rate of chlorination of magnesium oxide formed in situ from $MgCO_3$ added to a mechanically agitated bath of molten ternary salt in the temperature range 740 to 825 °C was controlled by the rate of CO transfer from the $CO/Cl_2/N_2$ mixed gas phase to the liquid phase. The rate of chlorination was measured for a number of impeller speeds, gas flow rates and gas compositions and correlated as:

$$\tilde{R}_{MgO} = 1.69x10^{-4}\left(\frac{P_{gassed}}{V_{liquid}}\right)^{0.35} v_g^{0.64} p_{CO}^{1.14}\ \frac{kmol}{m^3 s} \qquad (20)$$

Nomenclature

a	specific surface area m^2m^{-3}
C	molar concentration, kmol m^{-3}
d	diameter, m
d_b	equivalent spherical bubble diameter, m
D_l	liquid diffusivity, $m^2\ s^{-1}$
ΔG	Gibbs energy, kJ mol^{-1}
g	acceleration due to gravity, m s^{-2}
H	depth of molten bath, m
k_l	mass transfer coefficient, m s^{-1}

Published by Maney Publishing (c) Canadian Institute of Mining, Metallurgy and Petroleum

N	impeller speed, rpm
N_a	aeration number, $(Q/Nd^3_{impeller})$
N_{Ra}	Rayleigh number, $(d_b^3\Delta\rho g/D_l\mu)$
N_{Sh}	Sherwood number, $(k_l d_b/D_l)$
New	Weber number, $(\rho N^2 d_{impeller}^3/\sigma)$
P_{gassed}	gassed impeller power, W
$P_{ungassed}$	ungassed impeller power, W
p	gas activity, atm $(1\ atm)^{-1}$
Q	gas flow rate, $m^3\ s^{-1}$, STP
$\tilde{R}$	molar reaction rate, kmol $m^{-3}\ s^{-1}$
r	correlation coefficient
T	temperature, °C
V_l	volume of liquid in bath, m^2
v_g	superficial gas velocity, m s^{-1}

Greek symbols

ε	gas hold-uz
ρ	density, kg m^{-3}
σ	standard deviation
μ	viscosity, Pa s

Subscripts and superscripts

b	bulk
g	gas
l	liquid
x	dummy variable
y	dummy variab

REFERENCES

1. H.I. Kaplan, Magnesium Supply and Demand – 1994, Presented at IMA– 52, San Francisco, CA, May 23, 1995, Intl. Mag. Assoc., Washington, DC, 1995.

2. L.M. Pidgeon, New methods for the production of magnesium, Trans. Can. Inst. Min. Metall., Vol.47, 1944, pp.16-34.

3. M.P. Lugagne, The Magnetherm Process for the production of magnesium, Erzmetall, Vol.31, 1978, pp.310-313

4. Kh.L. Strelets, Electrolytic Production of Magnesium, Translated by J. Schmorak, Keterpress Enterprises, Jerusalem, Israel, 1977

5. N.Jarrett, Advances in the Smelting of Magnesium, Metallurgical Treatises, ed. by J.K. Tien and J.F. Elliot, METSOC AIME, Warrendale, PA, 1981, pp.159-169

6. G.J. Kipouros and D.R. Sadoway, The Chemistry and Electrochemistry of Magnesium Production, Advances in Molten Salt Chemistry 6, ed. by G. Mamantov, C.B. Mamantov, and J. Braunstein, Elsevier, Amsterdam, 1987, pp.127-109

7. M. Kennedy, Chlorination of Magnesium Carbonate in a Stirred Tank Reactor, M.Eng Thesis, McGill University, 1996

8. Annon., MagCan's new magnesium technology, Light Metal Age, June, 1990, p.20.

9. D.V. Pruttskov, V.N. Devyatkin, S.M. Lupinos, Ryabukhin, M. Yu. and V.G. Lysenko, Mechanics of magne site chlorination with a Cl_2 + CO mixture, Tsvetyne Metally (Soviet J. Non-ferrous Metals), May 1986, pp.52-56.

10. R.E. Treybal, Chapter 6: Equipment for gas-liquid operation, Mass Transfer Operations, 3rd ed., McGraw Hill, New York, NY, 1980, pp.139-219

11. M. Greaves and M. Barigou, Estimation of gas hold-up and impeller power in a stirred vessel reactor, Fluid Mixing III, Univ. Bradford, Sept. 8-10, 1987, Inst. Chem. Eng., Symp. Series No.198, 1987, pp.235-255.

12. J.C. Middleton, Chapter 17: Gas-liquid dispersion and mixing, Mixing in the Process Industries, N. Harby, M.F. Edwards and A.W. Nienow, eds., Butterworks, London, England, 1985, pp.322-355.

13. K. Van't Riet, Review of measuring methods and results in non-viscous gas-liquid mass transfer in stirred vessels, Ind. Eng. Process Des. Dev., Vol.18, No.3, 1979, pp.357-364.

14. J.G. Stevens and u, H., A computer model of a stirred tank reactor in trace alkaline elements removal from aluminum melt – The Alcoa Process, Light Metals, 1986, p.837.

15. H.B. Schultes, Baymag – high purity magnesium oxide from natural magnesite, CIM Bulletin, May, 1986, pp.43-47.

16. K. Koloini, I. Plazl and M.Zumer, Power consumption, gas hold-up and interfacial area in aerated non-Newtonian suspensions in stirred tanks of square cross-section, Chem. Eng. Res. Des., Vol.67, Sept. 1989, pp.526-36.

17. X.J.Guo, R. Li and R. Harris, , "Kinetics of Oxygen Transfer Through Molten Silver-Cupellation Slag", CMQ, Vol. 38, No.1, pp. 33-41, 1999

18. X. Qi and R.Harris, Effects of solids loading on cyanidation rates, Proc., 29th Ann. Meet. Canadian Mineral Processors., Feb., 1997, Ottawa, Ont., Can. Inst. Min. Metall. Pet., Montreal, QC, pp.325-340, 1997.

Published by Maney Publishing (c) Canadian Institute of Mining, Metallurgy and Petroleum

Published by Maney Publishing (c) Canadian Institute of Mining, Metallurgy and Petroleum